 SID, vol.1, no.4, pp.253-265, 2005

Fatigue Crack Growth Behaviour of Nitrided and Shot Peened Specimens

C. Colombo[1], **M. Guagliano**[12], **L. Vergani**[1]

Abstract: In this paper the fatigue crack growth properties of a nitrided and shot-peened steel is dealt with: different peening intensities were considered and the resulting residual stresses measured by means of an X-ray diffractometer. Rotating bending fatigue tests were executed on specimens including a blind micro hole, acting as a pre-existent crack. The fracture surface of broken specimens was observed with a SEM to detect the crack growth initiation point. The run-out specimens were broken after the test and the presence of non-propagating cracks detected. The results allowed to determine the propagation threshold of the nitrided and shot peened material.

keyword: Shot peening, Gas-nitriding, Residual stress, Fatigue threshold.

1 Introduction

The need of improved performances and more rational use of materials is making more and more popular the use of surface treatments to improve the mechanical behaviour of structural and machine elements [Marsh, 1993]. Among these treatments, shot peening is one of the most widely used, due to its ability in increasing the resistance to fatigue, fretting, rolling contact fatigue, stress corrosion cracking, etc.. The improved fatigue strength due to shot peening is mainly to be related with the residual stress induced by the action of the impact of the shot flow against the metallic surface. The effectiveness of the treatment can be strongly changed by using different peening parameters (shot material, dimension and velocity, that is to say by using different Almen intensities). Shot peening is generally applied as last treatment: in this way the modification of the residual stresses induced is prevented. Shot peening is generally applied after some hardening process, i.e. quenching and tempering, induction hardening, case hardening or carburizing. The effect of the application of carburizing and shot peening was very diffusely studied in the past, i.e. [Almen and Black, 1963], and [Guagliano, Guidetti and Riva, 2002], due to the fact that gears are one of the most important field of application of shot peening. Gears, in fact, are generally carburized to enhance their surface hardness and to improve their strength with respect of wear and rolling contact fatigue. Shot peening, furthermore, improves the behaviour of gears with respect of rolling contact fatigue and of bending fatigue at the gear tooth root.

However, carburizing requires high process temperature ($\sim$800 $^\circ$C), and induces geometrical distortion, making necessary further working processes: in the light of preventing this additional step, gear manufacturers are ever more considering nitriding as a possible substitute of carburizing. In fact, nitriding requires lower temperature ($\sim$530 $^\circ$C) and does not deform the gear teeth.

The effective depth of this latter treatment is lower than the one due to carburizing, even if the surface hardness increases, and the case/core transition depth is near to the one where there is the maximum tangential stress, according to Hertz theory. These considerations prevented for a long time the application of nitriding to gears and only recently this thermo-chemical treatment is becoming more and more used in gear power transmissions. In this light the application of shot peening should be useful to improve the performances of nitrided gears both as concern rolling contact fatigue and bending fatigue at the root of the tooth. The recent interest of gear manufacturers for nitriding can partially explain also the few reference data that is possible to find. In [Guanhua, Jawen and Naisai, 1991] the effect of shot peening on a low-alloy steel is analysed and the synergetic effect of the very hard layer due to nitriding and of the residual stress field induced by shot peening evidenced. In [Jingpu, 1984] the effect of shot peening on contact fatigue behaviour of 40Cr steel after a compound heat treatment that includes nitriding is analysed and the different failure modes un-

[1] Politecnico di Milano, Dipartimento di Meccanica

[2] Corresponding author: Tel.: 02.2399.8206; Fax.: 02.2399.8202; E-mail: mario.guagliano@polimi.it Extended version of the paper presented at the Conference "Fracture and Damage Mechnics IV", Mallorca, July 12-14, 2005

der different pressure values are underlined. From the S-N curves included in that paper, it is evident that shot peening has a positive effect on the fatigue behaviour of nitrided elements. Oshawa et al. [Ohsawa and Yonemura, 1984] studied the improvement of shot peening on gas-nitrided elements. They considered both glass beads and steel shots and were able to assess that shot peening increases the rotating bending fatigue limit of about 20%. Also the influence of the peening media and parameters on surface roughness was investigated.

In [Croccolo, and etc., 2002] the fatigue strength of a shot-peened nitrided low-alloy steel is investigated and the choice of the peening parameters is optimised by means of design of experiments. In this latter paper it is underlined that shot peening is useful only in the case of notched elements; in fact, if smooth ones are considered, shot peening is able to move the crack initiation point from the surface to a sub-surface inclusion with negligible improvement of the fatigue limit. As concern notched specimens, the fatigue crack starts sometimes from the surface and sometimes from an internal inclusion, depending on the applied load, on the thickness of the nitrided layer and on the choice of the peening parameters.

Indeed, the choice of the best treatment parameters is a complicated problem and only a quantitative and general model that considers residual stresses can orient the choice of the treatment parameters with the aim to obtain the most effective self-stress distribution in the hardened layer of material. In the case of nitrided materials the problem is even more complex due to the strong changing of the properties from the case to the core.

Starting from the well-known evidence that the residual stresses induced by shot peening are mainly effective in arresting crack propagation [8, 9], rotating bending fatigue tests were carried out on specimens including a micro-hole (depth equal to 0.080-0.150 mm), acting as a crack. Three series of specimens were considered: nitrided specimens, nitrided and shot peened (peening intensity 12A), nitrided and shot-peened (peening intensity 18A). This type of tests allowed to analyse the behaviour of the nitrided layer with respect of crack propagation and to assess the threshold value of ΔK of the nitrided layer and its variation with respect of the residual stress distribution. It was also possible to observe cracks starting from an internal inclusion and to relate this occurrence with the residual stress field. These latter were measured by using an X-ray diffractometer.

A finite element model of the cracked specimen was developed, with the aim to calculate the stress intensity factors, considering the residual stress effect.

Due to the long time required for model preparation and analyses a simple equation taken from literature was employed for the calculation of the stress intensity factors of several different crack depths.

2 Experimental tests

Sandglass shaped specimens were used for determining the fatigue strength of the treated material. The material used is 39NiCrMo3 (UTS=1053 MPa, Yield Strength=940 MPa, Elastic Modulus E=206000 MPa, Elongation A=20%). All the specimens were gas nitrided (temperature T=520 ° C, duration=50 h). Some of the specimens were then treated by peening characterized by intensity 12A and some by intensity 18A. In the central zone of all the specimens a micro-hole was realized by means of electro-erosion to introduce the presence of a like-crack defect, see Fig.1.

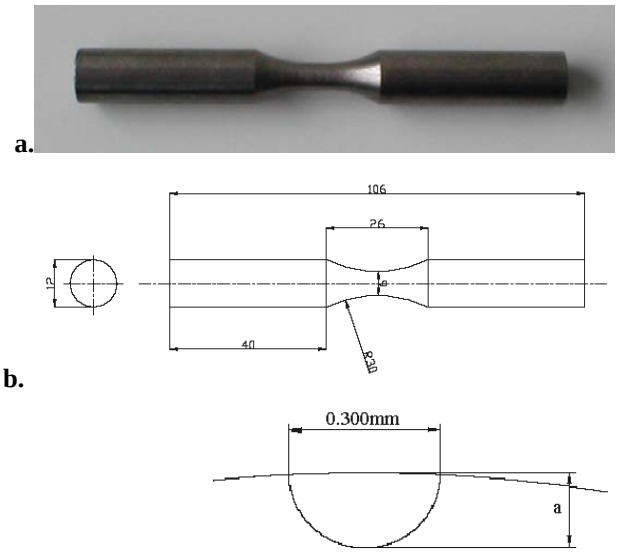

Figure 1 : a. Specimen used for the rotating bending fatigue tests; b. Specimen geometry c. Particular of the micro-hole.

The specimens have been divided in the following groups:

- nitrided, N (hole depth a≅0.150mm);

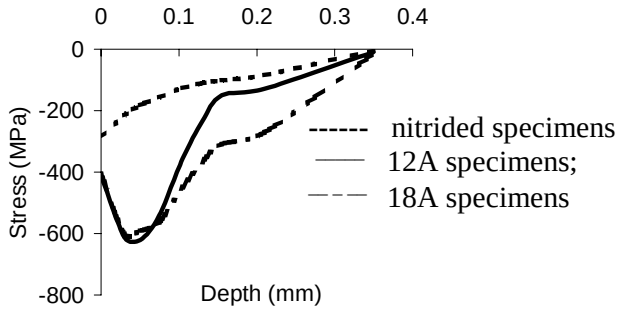

Figure 2 : Measured residual stress trends.

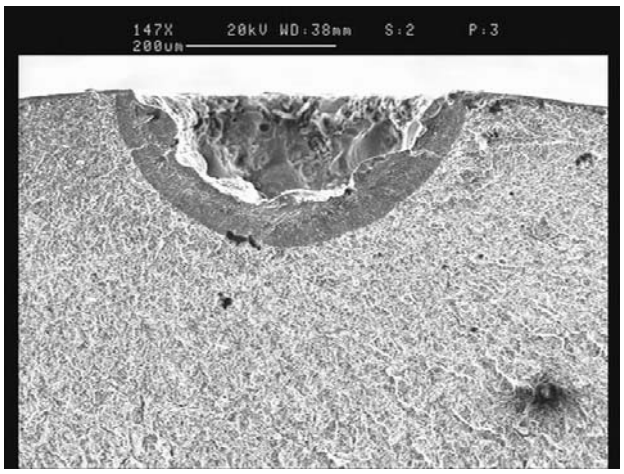

Figure 3 : An arrested crack found in a nitrided run-out specimen, σ_a=360 MPa.

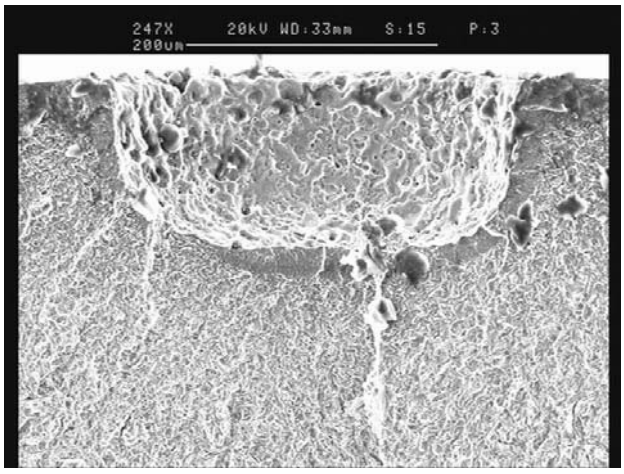

Figure 4 : An interrupted crack found in a 12A150 nitrided and peened run-out specimen, σ_a=660 MPa.

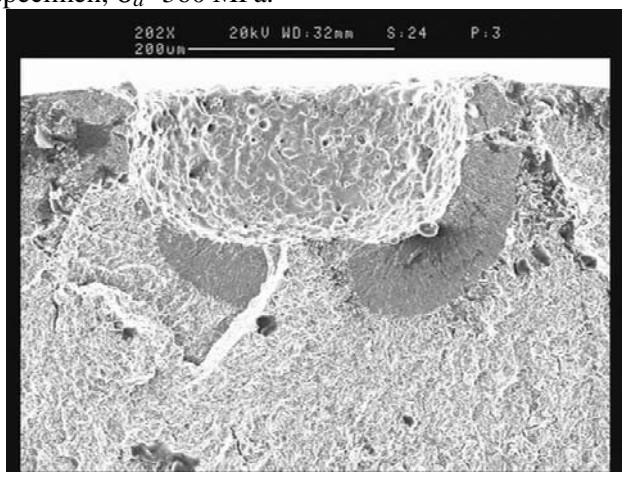

Figure 5 : An interrupted crack found in a 18A150 nitrided and peened run-out specimen, σ_a=760 MPa.

- nitrided and shot peened 12A100-12A150 (peening intensity: 12A, hole depth a≅0.080-0.100mm and 0.150mm);
- nitrided and shot peened 18A100-18A150 (peening intensity: 18A, hole depth 0.080-0.100mm and 0.150mm).

The residual stress values and trends, shown in Fig.2, were measured by using the X-ray diffraction technique. The residual stresses measurements were carried out by using a AST X3000 X-ray diffractometer (Cr radiation, Vn filter, $\sin^2\Psi$ method, 11 angles investigated): the irradiated area is about 1mm^2.

Rotating bending fatigue tests were experimentally carried out. The hole depth of nitrided specimens is always equal to 0.150 mm; on the contrary, the hole depth of shot peened specimens is variable. The effective depth, shown in the Tab.1, is experimentally measured when specimen fracture occurred in the section with the micro-hole. If the fracture occurred in different sections, it was not possible to measure the effective hole depth.

Tab.1 summarizes in details the results of all the experimental tests, in terms of stress amplitude, σ_a, depth of the micro-hole and inclusions. Tests have been carried out for the maximum duration of $2{\cdot}10^6$ cycles: over this value, the specimen has been classified as run-out.

Shot peened specimens were divided in two groups: the first one considers micro-hole depths $a \leq 0.100$ mm, the second one considers micro-hole depths $a > 0.100$ mm. Results and fatigue strength determined by the accelerated stair case method [Dixon and Massey, 1983] are reported in Tab.2: the improvement induced by shot peen-

Table 1 : Experimental results for all the analysed specimens. (For peened specimens, crack propagation started from M = micro-hole, I = inclusion)

a.

Nitrided specimens (N) a=0.150mm			
test	**σ_a[MPa]**	**result**	**n ° cycles**
1	360	run-out	$>$ 2000000
2	380	run-out	$>$ 2000000
3	400	broken	300984
4	380	broken	184272
5	360	run-out	$>$ 2000000
6	380	broken	299693
7	360	run-out	$>$ 2000000
8	380	broken	233327
9	360	run-out	$>$ 2000000

b.

Nitrided and 12A shot peened specimens (12A100)						
test	**σ_a[MPa]**	**result**	**n ° cycles**	**a[mm]**	**depth of inclusion[mm]**	**composition of inclusion**
1	740	run-out	$>$ 2000000	0.080	/	
2	760	broken (I)	1012280	/	0.415	Al, Pb
3	740	broken (I)	1800116	/	0.376	Ca, Pb
4	720	run-out	$>$ 2000000	n.a.	/	
5	740	run-out	$>$ 2000000	0.080	/	
6	760	broken (I)	1992351	/	0.675	Al
7	740	broken (I)	807645	/	0.344	Al, Pb
8	720	run-out	$>$ 2000000	/	0.460	/
9	740	run-out	$>$ 2000000	n.a.	/	
10	760	run-out	$>$ 2000000	0.085	/	
11	780	broken (M)	129153	0.100	/	
Nitrided and 12A shot peened specimens (12A150)						
test	**σ_a[MPa]**	**result**	**n ° cycles**	**a[mm]**	**depth of inclusion[mm]**	**composition of inclusion**
12	660	run-out	$>$ 2000000	0.150	/	
13	680	broken (M)	255657	0.150	/	
14	660	run-out	$>$ 2000000	0.150	/	
15	680	broken (M)	111001	0.150	/	
16	660	run-out	$>$ 2000000	n.a.	/	

c.

Nitrided and 18A shot peened specimens (18A100)						
test	σ_a**[MPa]**	**result**	**n ° cycles**	**a[mm]**	**depth of inclusion[mm]**	**composition of inclusion**
1	780	broken (I)	545000	/	0.570	Pb
2	760	broken (I)	1230000	/	0.559	Pb
3	740	broken (I)	1204000	/	0.454	Al
4	720	run-out	$>$ 2000000	n.a.	/	
5	740	broken (I)	933000	/	0.661	Pb
6	720	broken (I)	977000	/	0.347	Pb
7	700	run-out	$>$ 2000000	n.a.	/	
8	720	run-out	$>$ 2000000	n.a.	/	
9	740	broken (I)	1729000		0.534	Al, Mn, Pb
10	720	run-out	$>$ 2000000	n.a.	/	
Nitrided and 18A shot peened specimens (18A150)						
12	760	run-out	$>$ 2000000	n.a.	/	
13	780	broken (I)	1222836	/	0.433	S, Mn
14	760	run-out	$>$ 2000000	0.150	/	
15	780	broken (I)	375401	n.a.	/	
16	760	broken (M)	191353	0.150	/	

Table 2 : Accelerated stair-case results.

Specimen type	**Bending fatigue strength [MPa]**	**Notes**
Nitrided N	379	The fractures begin from holes
Shot peened 12A100	748	The fractures begin from holes and inclusions
Shot peened 12A150	674	The fractures begin from holes
Shot peened 18A100	762	The fractures begin from inclusions
Shot peened 18A150	724	The fractures begin from holes and inclusions

ing is evident.

By looking at the results, it is interesting to note the different fatigue behaviour of the specimen groups. In the case of the N and 12A150 specimens the fatigue cracks always start from the hole and some interrupted cracks were evidenced in run-out specimens, broken after the end of the test and observed by means of a SEM. The extension and the shape of interrupted cracks found in the nitrided and shot peened specimens are shown in Fig. 3, 4, 5.

The 12A100 and 18A150 specimens, on the contrary, broke by cracks initiating both from internal inclusions and holes, while 18A100 specimens broke only from inclusions.

The different fatigue behaviour is correlated to the residual stress patterns. In fact it is possible to note from Fig.2 that at the hole bottom the corresponding compressive residual stress values in the case of N and 12A150 specimens are lower than in the case of 12A100 and 18A150, while it is possible to underline that for 18A100 specimens residual stress are the highest ones. Moreover it is important to note that the surface distance where internal inclusions are placed, from which cracks propagate, corresponds to the tensile residual stress zone.

These different modes of failure are an index of the ability of residual stresses in preventing crack propagation in the nitrided material. Moreover, the depth at which the residual stresses change sign could be considered an

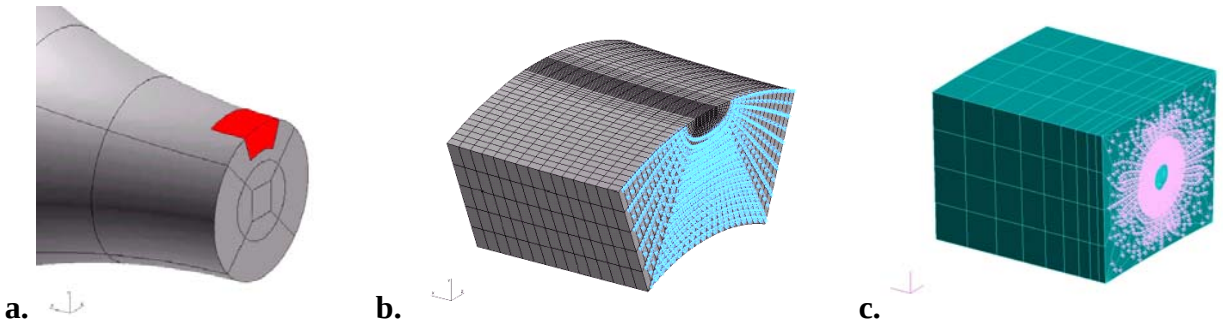

Figure 7 : a. Particular of the global model and extraction of the first sub-model; b. First sub-model with semi-elliptical crack; c. Second sub-model with circular crack.

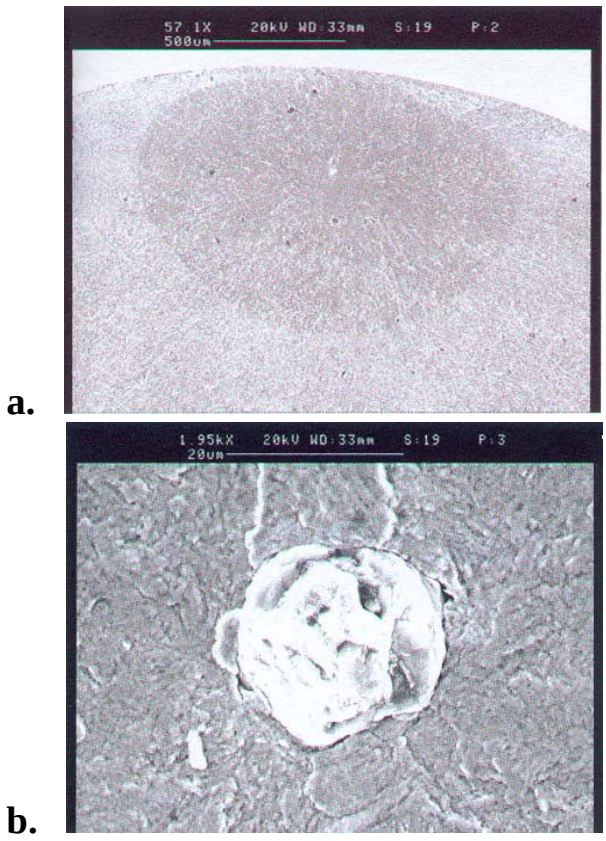

Figure 6 : Crack in a 18A150 specimen beginning from an inclusion.

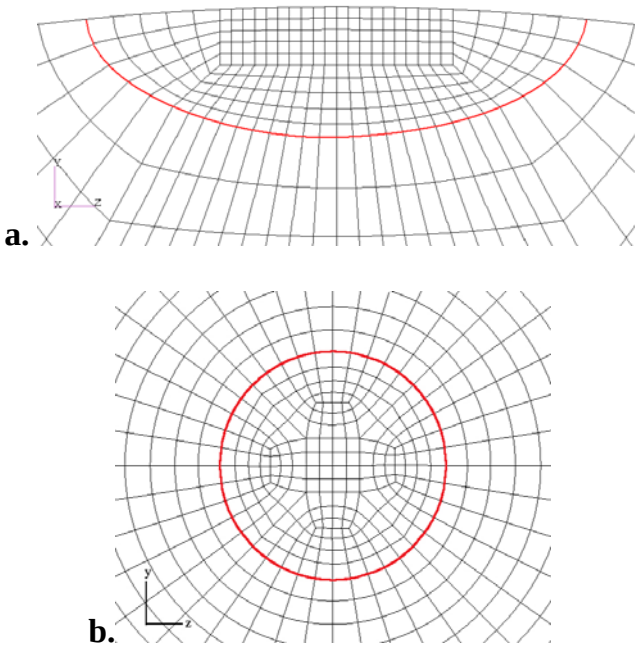

Figure 8 : Particular of the mesh of the two sub-models in the cracked zone.

index to evaluate the optimal peening parameters, by relating it with the depth and the dimension of typical inclusions of this material.

12A100 and 18A specimens have shown a similar behaviour, because they present a compressive residual stress profile larger with respect of the other samples in correspondence of hole bottom. For all these specimens, the crack started from inclusions (diameter≈0.020 mm) at an average depth of 0.52 mm, that is in the tensile residual stress area. Propagation of a crack and the shape of an inclusion are shown in Fig.6.

3 Effective stress intensity factor calculation

A three-dimensional finite element model of the cracked specimens was realized by following the sub-modelling approach and by including the presence of the residual stresses [Hibbit, Karlsson and Sorensen, 2001].

The global model of the specimen is shown in Fig.7a:

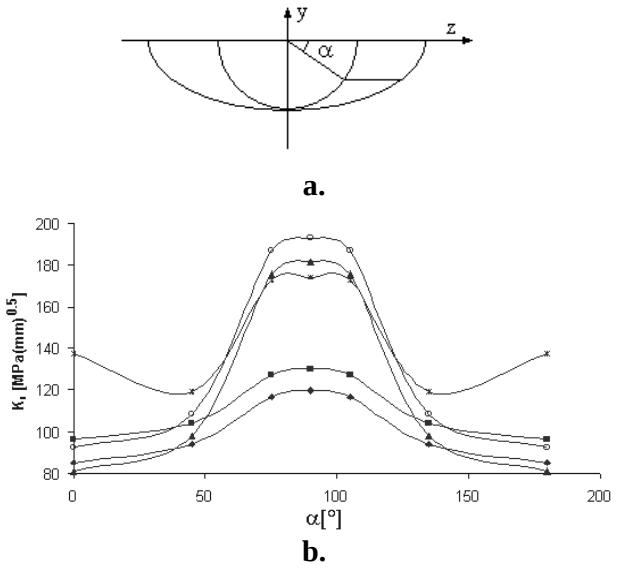

Figure 9 : a. definition of the angle α along the crack front; b. K_I values along the semi-elliptical crack front: −♦− N specimen, broken, σ_a = 380MPa; −■− N specimen, run-out, σ_a = 360MPa; −▲− 12A150 specimen, broken, σ_a = 680MPa; −◯− 12A150 specimen, run-out, σ_a = 660MPa; −∗− 18A150 specimen, broken, σ_a = 760Mpa

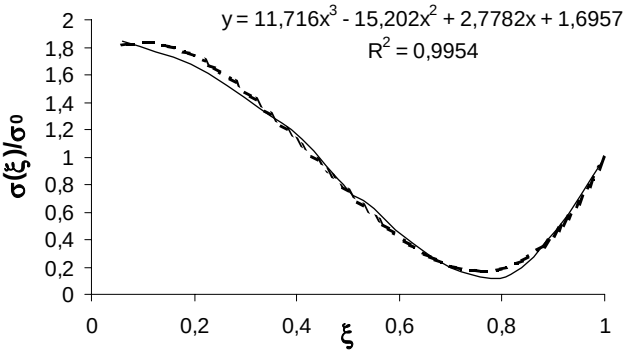

Figure 10 : Example of a third order interpolation for a 12A150 specimen with σ_a=680 MPa (− effective normalised stress, - - - interpolation).

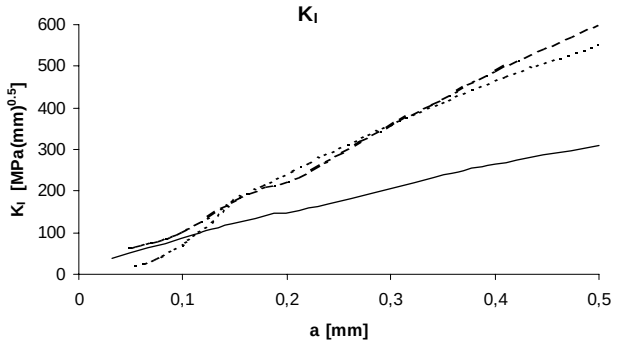

Figure 11 : K_I values for different depths (a) of the semi-elliptical crack: − N, σ_a=360 MPa; - - - 12A, σ_a =660 MPa; − - - 18A, σ_a =760 MPa.

due to the load and geometry symmetry only one half is considered. Two sub-models were realized, the first one, reported in Fig.7b schematises the micro-hole. The crack front is an arc of an ellipse. The second one (Fig.7c) schematises an inclusion as a circular crack. The meshes of the sub-models are shown in Fig.8.

The load applied to the global model is the bending moment acting on the symmetry plane of the crack. The displacements calculated by the global model are used as boundary conditions on the free surfaces of the sub-models. The stress intensity factor, K_I, was calculated along the crack fronts, according to the indications in [Zhu, Liu and Chao, 2001] and [Kassir and Sih, 1966].

K_I values are calculated by using crack opening displacements obtained from FE analysis. Some results related to the surface crack are shown in Fig.9, as a function of the angle α defined in Fig.9a.

Due to the symmetry of the load the values are symmetrical with respect of the crack axis.

However, the FE model is time-consuming, both as regard modelling and computational time: with the aim to analyse different crack depths a simpler approach is adopted.

This approach considers the equations included in [Murakami, 1987] to obtain the SIF values of different crack depths. Also the different residual stress fields induced by shot peening (N, 12A and 18A) are introduced. A third order interpolation of the stress profile as function of the depth, correctly approximates the effective stress pattern due to the bending moment and the residual stresses.

Fig.10 shows an example of this interpolation: effective stress is normalised with respect of the surface stress, expressed as function of the coordinate ξ defined as:

$$\xi = 1 - \frac{y}{a} \tag{1}$$

where y is the radial coordinate starting from surface and

a is the considered crack depth. A R^2 parameter near to 1 allows to confirm the goodness of the results.

The K_I values, calculated as shown in Appendix, are in good agreement with the ones obtained from FE analysis, with an error lower than 7%. Using this model, other values of K_I were found for different depths of the semi-elliptical crack, obtaining the trends shown in Fig.11. In this figure it is possible to see the influence of different compression residual stress on the surface of specimens on SIF values, as function of a, the depths of the crack.

Table 3 : K_I values (σ_a = 760 MPa, 18A).

a. internal circular cracks

inclusion diameter [mm]	**distance from the surface [mm]**	**K_I [MPa$\sqrt{\text{mm}}$]**
0.020	0.520	71
0.030	0.520	87
0.040	0.520	101
0.030	0.400	91

b. semi - elliptical cracks

depth of semi-elliptical cracks [mm]	**K_I [MPa$\sqrt{\text{mm}}$]**
0.080	83
0.085	87
0.100	103
0.150	179

From the diagram of Fig.11 is evidenced the strong influence of the relative position of the crack tip with respect of the residual stress field on the stress intensity factor.

For the second FE sub-model, simulating the circular crack propagated from an inclusion out of the compressed material, numerical analysis were focused on 18 Almen peened specimens.

Tab.3a summarises the results related to the internal cracks, simulating the inclusions positioned in the average (0.520 mm) and minimum (0.400 mm) surface distance observed in the fractured specimens. The diameter of the inclusions was varied from 0.020 to 0.040 mm to simulate the propagation of the crack. Tab 3b summarises the stress intensity values obtained for semi-elliptical cracks.

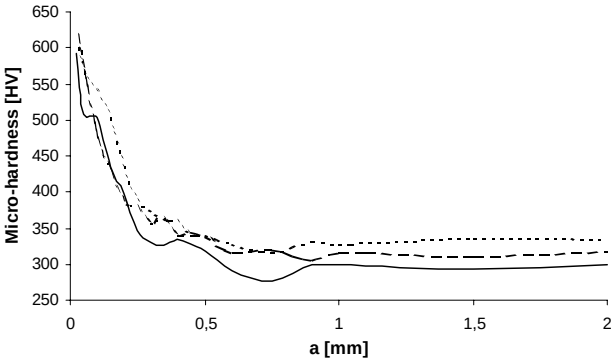

Figure 12 : Micro-hardness profiles: — N, - - - 12A, and – – – 18A (100 g, t=15 s).

The applied stress (σ_a= 760 MPa) and the residual stresses are the same for both the cracks considered, being the aim to evaluate the criticality of surface defects with respect of material ones.

The stress intensity factors obtained by the two different cases are similar, thus justifying the experimental results. In the case of a surface crack 0.150 mm depth, the stress intensity factor is strongly larger than the one related to inclusions, according to the experimental evidence. In Tab.1, only in this case the 18A specimen is fractured from the micro-hole.

4 Threshold stress intensity factor determination and comparison with experimental results

An approximated value of the threshold stress intensity factor ΔK_{th} is evaluated, for the three analysed cases. ΔK_{th} was obtained following the approach proposed in [Murakami and Endo,1994]:

$$\Delta K_{th} = 3.3 \cdot 10^{-3} (HV + 120) \left(\sqrt{area}\right)^{1/3} \left[MPa\sqrt{m}\right] \quad (2)$$

where $\sqrt{\text{area}}$ is in μm and HV is micro-hardness in Vickers.

This formula relates ΔK_{th} to Vickers micro-hardness on the defect tip, as the representative parameter of material micro-structural characteristics. Micro-hardness was experimentally determined, and the profiles in Vickers units are shown in Fig.12 for each surface treatment.

The geometrical parameter used by [Murakami and Endo,1994] to represent the influence of form and dimension of crack in defining ΔK_{th} is the square root of

area, obtained by projecting a small defect or crack onto a plane perpendicular to the maximum principal stress. The $\sqrt{\text{area}}$ parameter allows to uniform the behaviour of small cracks, inclusions and crystalline inclusions, comparing it to the micro-crack one.

The method of [Murakami and Endo,1994] is worthy for a large class of materials and defects, with the parameter $\sqrt{\text{area}}$ included between 50 and 1000 μm. Over this upper limit, the proposal formulas are not employable, because the micro-cracks behaviour tends to the long cracks one.

However, this formula was not proposed for surface hardened steels; moreover, for the peened specimens, it must be considered the presence of compression residual stress on the surface. For these reasons, the proposal relation [Murakami and Endo,1994] is:

$$\Delta K_{th} = 3.3 \cdot 10^{-3} (HV + 120) \left(\sqrt{area}\right)^{1/3} \times \left(\frac{1-R}{2}\right)^{\left(0.226+HV \cdot 10^{-4}\right)} \left[MPa\sqrt{m}\right] \quad (3)$$

using different stress ratio R as function of the considered depths, because of the presence of residual stress which influences the stress profile. R was calculated as follows:

$$R = \frac{\sigma_{\min}}{\sigma_{\max}} = \frac{-\sigma_a + \sigma_{res}}{\sigma_a + \sigma_{res}} \quad (4)$$

considering that σ_a is the bending applied stress on the crack tip, and σ_{res} is the compression residual stress induced by nitriding and shot peening. Also microhardness and $\sqrt{\text{area}}$ were varied in function of the considered crack depths.

The obtained results of ΔK_{th} as function of the crack depth are graphically proposed in Fig.13. The ΔK_{th} profiles obtained both from eq. (2) and (3), for N specimens, 12 and 18 Almen peened ones, as function of crack depth, a, in the compressed layer of material (a = 0.350 mm). As it is possible to see in these diagrams, by applying the two proposed formulas, the ΔK_{th} profiles are strongly different close to the surface, where the influence of residual stress is considerable and highly modifies the R ratio.

In the same figure, ΔK values obtained in the cases of 0.150 mm crack depth are shown; ΔK is calculated by considering the stress range ($\sigma_{max} - \sigma_{min}$). A ΔK value ($\circ$) is related to the run out specimen while the other ($\bullet$) is related to the broken specimen.

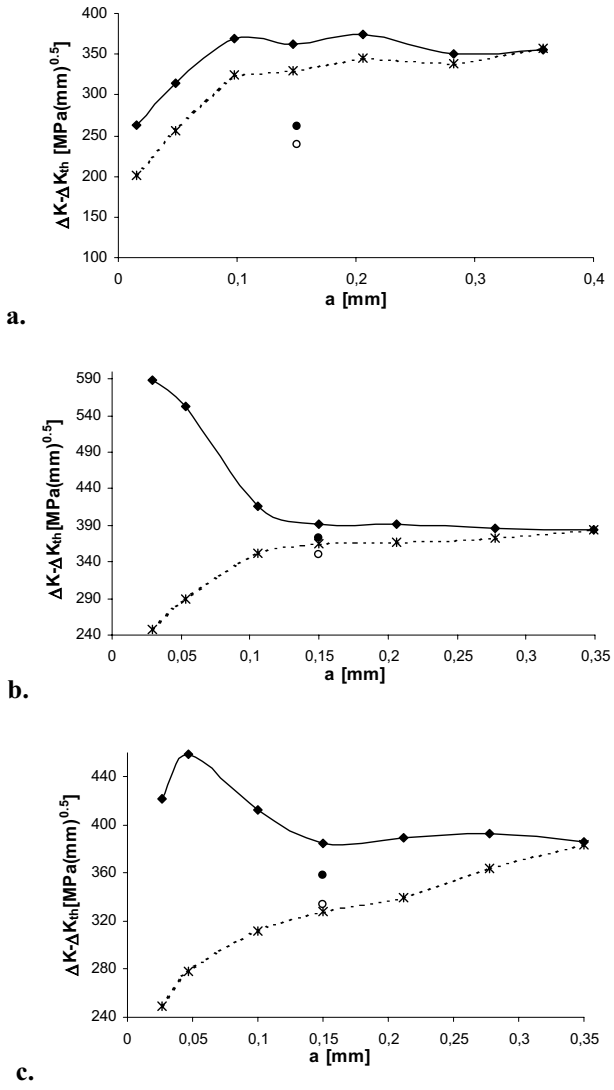

Figure 13 : Comparison between expected values of ΔK_{th} calculated from eq. (2) —∗— and from eq. (3) −♦− and ΔK values obtained from numerical analysis for broken ($\bullet$) and run-out ($\circ$) specimens, for N (a.), 12A (b.) and 18A (c.) specimens. (comparison depth of the micro-hole: 0.150 mm)

Explicit values referred to a = 0.150 mm are shown in Tab.4.

The approach seems well describing the experimental tests, especially for peened specimens, even if the comparison is related only to two specimens and it would be a larger experimentation. The calculated values are close to the threshold ones even if they do not allow to accurately predict the condition of propagation.

Table 4 : Values of ΔK and ΔK_{th} obtained for crack depth of 0.150 mm. (ΔK_{th} for peened specimens are calculated * from eq. (2) and ** from eq. (3))

Specimen	**Applied stress** σ_a [MPa]	ΔK $\left[\text{MPa}\sqrt{\text{mm}}\right]$	ΔK_{th} $\left[\text{MPa}\sqrt{\text{mm}}\right]$	
N	360 (run-out)	239	330*	362**
	380 (broken)	260		
12A	660 (run-out)	349	346*	392**
	680 (broken)	373		
18A	740(run-out)	358	328*	384**
	760 (broken)	334		

Due to the strong importance of the residual stresses in determining the ΔK_{th}, the definition of R in equation (3) is critical and should be based on the residual stress pattern and not on the local values.

To looking depth at this point further analyses are necessary and will be performed.

5 Conclusions

The following results are found from tests carried out on cracked nitrided and shot peened specimens:

1. the fatigue behaviour is strictly correlated with the residual stress pattern;

2. the location of the crack initiation point can lay on the surface or at an internal inclusion, depending on the applied stress and on the position of the inclusion with respect of the residual stress field;

3. the application of a literature relation permits the calculation of the effective stress intensity factor;

4. by comparing the numerical results with experimental tests, it is possible to assess the value of the threshold stress intensity factor ΔK_{th}, through two parameters, micro-hardness and $\sqrt{\text{area}}$, which summarize material and crack behaviour. However, further work is necessary to better understand the effect of R, including the effect of the residual stress field.

References

Marsh, K.J. (1993): Shot Peening: Techniques and Applications. *EMAS, London*.

Almen, J. O.; Black, P.H. (1963): Residual stresses and fatigue in metals. *McGraw-Hill Book Company.*

Guagliano, M; Guidetti, M.; Riva, E. (2002): Contact fatigue failure analysis of shot peened gears. *Engineering Failure Analysis,* vol. 9, pp. 147-158.

Guanhua, D.; Jawen, H.; Naisai, H. (1991): The effect of shot peening on the residual stress and fatigue property of nitrured layer of 42CrMo steel. 5^{th} *Annual Conference of CMES HTI*, Tianjin (China).

Jingpu Z. (1984): Effect of shot peening on contact fatigue behaviour of 40Cr steel after compound heat treatment. *Proceedings of the II International Conference on Shot Peening* (ICSP2), Chicago (USA), pp. 215-224.

Ohsawa, M.; Yonemura, T. (1984): Improvement of hardened surface by shot peening. *Proceedings of the II International Conference on Shot Peening* (ICSP2), Chicago (USA), pp. 147-158.

Croccolo, D.; Cristofolini, L.; Bandini, M.; Freddi, A. (2002): Fatigue strength of shot peened nitrided steel: optimization of process parameters by means of design of experiment. *Fatigue and Fracture of Engineering Materials and Structures*, vol. 25, pp. 695-707.

Song, P.S.; Wen, C.C. (1999): Crack closure and crack growth behaviour in shot peened fatigued specimen. *Engineering Fracture Mechanics*, vol. 63, pp. 295-304.

Guagliano, M. (2001): Relating the Almen intensity to residual stresses induced by shot peening: a numerical approach. *Journal of Material Processing Technology*, vol. 110, pp. 277-284.

W.J. Dixon; F.J. Massey (1983): Introduction to statystical analysis. *McGraw-Hill*.

Hibbit, Karlsson & Sorensen Inc (2001):

Abaqus/Standard User's Manual (version 6.2), Vol. I, II, III.

Zhu, X.K.; Liu, G.T.; Chao, Y.J (2001): Three dimensional stress and displacement fields near an elliptical crack front. *International Journal of fracture*, vol. 109, pp. 383-401.

Kassir, M.K.; Sih, G.C (1966): Three-dimensional stress distribution around an elliptical crack under arbitrary loadings. *Journal of Applied Mechanics*.

Murakami, Y. (Ed.) (1987): Stress Intensity Factors Handbook. *Pergamon Press*, vol. II, pp. 725-727.

Murakami, Y.; Endo, M. (1994): Effects of defects, inclusions and inhomogeneities on fatigue strength. *International Journal of Fatigue*, vol. 16, pp. 163-182.

Appendix A: Calculation of K_I.

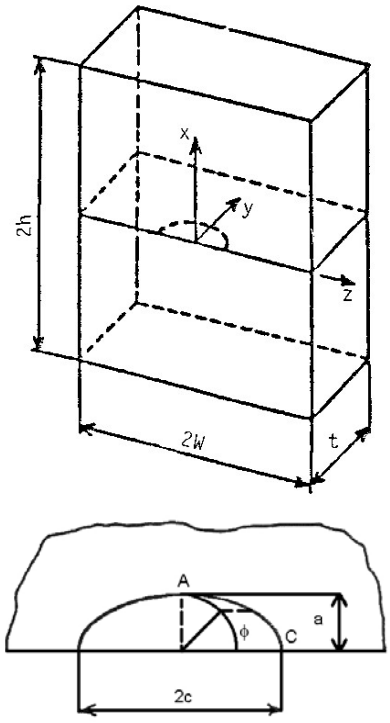

Figure 14 : Definition of point A and shape of the crack.

The calculation of the stress intensity factors of the semi-elliptical crack is developed following [Murakami, 1987], without considering the specimen bending, but assuming the crack in a plate under basic mode of stress distribution. The interpolation of the effective stress on crack surface, in function of the coordinate ξ, as defined in eq. (1), allows to obtain four constants, A, B, C and D, related to the principal stress distributions:

$$\sigma(\xi) = \left(A\xi^3 + B\xi^2 + C\xi + D\right) \cdot \sigma_0 \tag{5}$$

An example is shown in Fig.10. σ_0 is the surface stress, equal to:

$$\sigma_0 = \sigma_a + \sigma_{res} \tag{6}$$

Global K_I is defined as sum of K_i, related to the stress distributions:

$$K_I = AK_3 + BK_2 + CK_1 + DK_0 \tag{7}$$

where A, B, C and D are the constants determined in the interpolation of the stress in (5). Tab.5 shows a summary of the different analysed stresses.

K_i is defined as:

$$K_i = \frac{M}{\Phi}\sigma_0\sqrt{\pi a} \tag{8}$$

Table 5 : Analyzed distribution of stress.

Stress	$\mathbf{K}_i$
$\frac{\sigma(\xi)}{\sigma_0} = 1$	K_0
$\frac{\sigma(\xi)}{\sigma_0} = \xi$	K_1
$\frac{\sigma(\xi)}{\sigma_0} = \xi^2$	K_2
$\frac{\sigma(\xi)}{\sigma_0} = \xi^3$	K_3

Table 6 : Values of M for the analysed crack shape.

$\mathbf{M}_i$	**point A**
M_0	1.1045
M_1	0.409
M_2	0.2445
M_3	0.173

where Φ is function of the ratio a/c, the characteristic dimensions of the crack (a=0.150 mm and a/c=2).

$$\Phi = \begin{cases} E(k),\ k = \sqrt{1 - \frac{a^2}{c^2}}\ a \le c \\ \left(\frac{a}{c}\right) E(k'),\ k' = \sqrt{1 - \frac{c^2}{a^2}}\ c \le a \end{cases} \tag{9}$$

Table 7 : Values of M in [Murakami, 1987]

$\mathbf{M}_0$					
a/c	Point	a/t			
		0.2	0.4	0.6	0.8
0.2	A	1.162	1.371	1.651	1.787
	C	0.582	0.688	0.882	1.201
0.4	A	1.119	1.216	1.327	1.379
	C	0.810	0.911	1.060	1.320
0.6	A	1.090	1.143	1.206	1.228
	C	0.954	1.025	1.192	1.366
1	A	1.047	1.083	1.106	1.107
	C	1.145	1.220	1.318	1.441
$\mathbf{M}_1$					
a/c	Point	a/t			
		0.2	0.4	0.6	0.8
0.2	A	0.490	0.610	0.795	0.863
	C	0.502	0.578	0.718	0.945
0.4	A	0.435	0.490	0.563	0.576
	C	0.678	0.750	0.850	1.039
0.6	A	0.383	0.418	0.457	0.449
	C	0.795	0.840	0.960	1.091
1	A	0.304	0.330	0.342	0.327
	C	0.960	1.010	1.080	1.174
$\mathbf{M}_2$					
a/c	Point	a/t			
		0.2	0.4	0.6	0.8
0.2	A	0.309	0.400	0.539	0.584
	C	0.447	0.509	0.620	0.796
0.4	A	0.264	0.310	0.369	0.373
	C	0.593	0.650	0.729	0.874
0.6	A	0.225	0.257	0.288	0.277
	C	0.692	0.727	0.823	0.927
1	A	0.170	0.189	0.200	0.183
	C	0.842	0.879	0.934	1.011
$\mathbf{M}_3$					
a/c	Point	a/t			
		0.2	0.4	0.6	0.8
0.2	A	0.226	0.300	0.412	0.445
	C	0.405	0.459	0.553	0.695
0.4	A	0.188	0.229	0.277	0.278
	C	0.531	0.579	0.641	0.763
0.6	A	0.158	0.187	0.213	0.202
	C	0.618	0.647	0.727	0.814
1	A	0.117	0.134	0.143	0.127
	C	0.756	0.785	0.832	0.896

In the analysed crack, it is used the first part of eq. (9), and the function E(k) has the following value:

$$\Phi = E(k) = \sqrt{1 + 1.464 \left(\frac{a}{c}\right)^{1.65}} = \quad 1.227 \qquad (10)$$

The constant M is obtained from the interpolation of values proposed in tables in [Murakami, 1987] in function of the crack geometry, and proposed in Tab.7. The interpolation gives the values shown in Tab.6, presented only for point A, where there is the maximum K_I value, according to the numerical analysis. The position of A is defined in Fig.14. The value of t, depth of the plate, is assumed equal to the specimen diameter (6 mm).